Simulation of colloidal crystallization on finite structured templates

A. Cacciuto and D. Frenkel

FOM Institute for Atomic and Molecular Physics, Kruislaan 407, 1098 SJ Amsterdam, The Netherlands

We present a numerical study of colloidal crystal growth on finite templates. Specifically, we consider planar, crystalline templates with the structure of the **100**, **110**, and **100** faces of a fcc crystal. We explore how the size of the induced crystallites depends on template area, lattice spacing and degree of supersaturation. We find that thermal fluctuations of the templating particles around their average positions have a strong effect on the size of the crystallites that grow epitaxially. If the fluctuations exceed the Lindemann criterion, the templates cease to function as a crystallization seed. We find that our numerical results are well described by a suitably modified version of classical nucleation theory.

I. INTRODUCTION

The ability to control the structure, size, and orientation of colloidal crystals is of considerable technological importance, as such crystals could be applied as switches [1], optical filters [2–4] and as photonic band gap materials [5,6]. It is, however, difficult to generate large single crystals of the desired structure and orientation. Experiments by van Blaaderen *et al.* [7] showed that high-quality colloidal crystals could be grown using template-driven crystallization. The experiments of Ref. [7] have inspired much experimental and numerical work [8–14]. Most numerical studies consider crystallization on infinite (strictly speaking, periodically repeated) crystal planes that are commensurate with the simulation box. Recently, it has become possible to perform experiments on crystallization induced by two-dimensional templates of arbitrary structure, using arrays of colloidal particles trapped by multiplexed optical tweezers [15]. In such experiments, only a relatively small number of particles, N_T, can be trapped by the tweezers. Typical templates in dense solutions consist of about 100 particles (however 20×20 templates have been generated in low-density solutions [16]). Limiting factors are the effective optical trap stiffness k_{eff} felt by each particle in the template and the overall size of the window the laser beam can span. k_{eff}, decreases with the number of particles trapped and if k_{eff} is not sufficiently large, thermal fluctuations can drastically reduce the ability of the template to induce crystallization in the sample. Moreover, constructing the templates is not easy, tracer particles that have a slightly different index of refraction than the solution must be located and incorporated in the template. This is a laborious work which requires some care, as no trap should contain more than one particle.

In this paper, we report Monte Carlo simulations that consider template-induced crystallization on finite templates of sizes comparable to those used in experiments. We performed Monte Carlo simulations on a system of spherical particles in the presence of a finite planar template with particles arranged in a square or hexagonal lattice. The position of the particles in the template is set in the *x-y* plane. All spheres have the same diameter, σ, and interact via a hard-core potential. The total number of particles in the system was $N=7776$ (including the ones in the template which are

maintained fixed at their lattice positions at all times). All simulations were carried out in the NP_zT ensemble, where P_z denotes the diagonal component of the pressure tensor perpendicular to the template.

The geometry of the simulation box was rectangular with periodic boundary conditions. The side length in the *x* and *y* direction was fixed to $L_x=18a$ and $L_y=18a$ (where a is the lattice spacing of the template), while the height of the box L_z was adjusted to accomodate the system constant external pressure P_z. Throughout the paper all length scales are normalized by the diameter of the particles σ.

We systematically explored how symmetry, size, template lattice spacing and supersaturation of the solution affect the ability of the templates to induce crystallization. Specifically we investigated templates with particles arranged according to **111**, **110**, and **100** faces of an fcc crystal (see Fig. 1).

II. METHODS

One should be careful when quantifying the ability of the different templates to induce crystallization as different templates may favor different crystal structures. Our analysis of crystal formation should be unbiased, i.e., we should be able to detect all relevant crystal structures. To achieve this, we considered several possible order parameters. To identify crystalline layers, it is usually convenient to use a two-dimensional bond-order parameter,

$$\psi_n(i) = \frac{1}{N_b} \sum_{k=1}^{N_b} e^{in\theta_{ik}}. \tag{1}$$
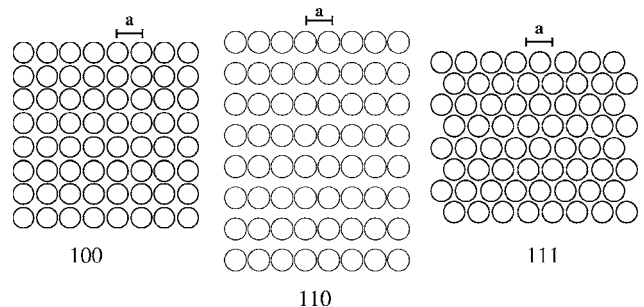
FIG. 1. Sketch of **100**, **110**, and **111** templates.
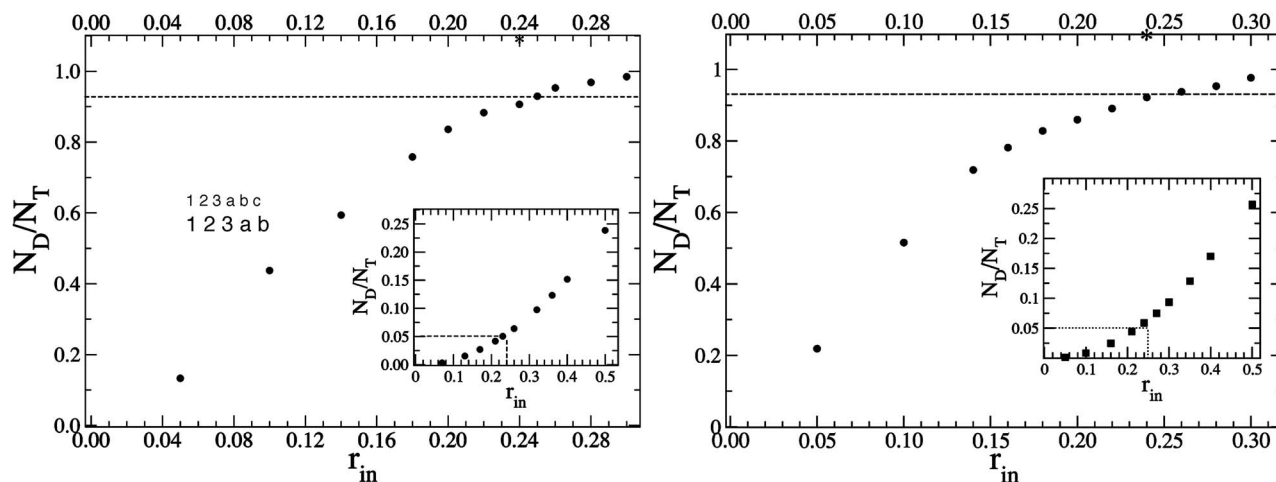
FIG. 2. Average number of crystalline particles on the first layer of the template detected by the order parameter, N_D, divided by the total number of particles in the template N_T as a function of r_{in}. The image on the left-hand side refers to the **111** template, while the image on the right-hand side refers to the **100** template. Insets show the same analysis done on particles disposed at random in the first layer of the template. In both cases we used templates of 64 particles. The lattice spacing is taken to be $a = 1.11\sigma$ for both templates.

To detect crystal growth on square (**100, 110**) and triangular (**111**) substrates, it is logical to use $\psi_4(i)$ and $\psi_6(i)$, respectively. However, we are not simply interested in detecting crystal growth. Rather, we wish to compare in an unbiased way, the relative efficiency of different templates to induce crystalline ordering and, for such a quantitative comparison, we found it inconvenient to use the above bond-order parameters. An alternative would be to use a single bond-order parameter that would detect both square and hexagonal patterns [e.g., $\psi_{12}(i)$]. However, we also found this order parameter to be computationally inconvenient (noisy). We also considered three-dimensional bond-order parameters [17], but these are less practical for this specific application than the method we describe below. In bulk systems, bond-order parameters are used to detect crystallites in an otherwise isotropic system. However, in the present system, the symmetry is already broken and we know where to expect the next crystalline layer to form. This allows us to determine the number of crystalline particles as follows: first, we determine the location of the (incipient) crystal planes that form parallel to the template. This is done by finding the peaks in the distribution function $g(z)$, where z denotes the perpendicular distance from the plane of the template. We then tag a particle as *crystalline* if its coordinates projected in the nearest crystal plane lie within a circle of radius r_{in} from the closest predetermined lattice site. The cutoff r_{in} is adjusted as follows: we first compress the system to a density at which the first layer covering the template is fully crystalline (this can be checked by imaging the particles). The value of r_{in} is then chosen such that the prepared layer is recognized as crystalline. If r_{in} is too small, only few particles in the first layer will be detected as crystalline. Increasing r_{in} the number of solidlike particles N_S will increase and eventually level off. As both sides of the templates that we consider are exposed to the solution, crystallites can grow on both sides. Throughout this paper, N_S denotes the average of the sizes of the crystallites on both sides of the template, $N_S = (N_S^{Up} + N_S^{Down})/2$. If r_{in} is chosen too large, disordered layers

will be identified as crystalline. Hence, we should choose r_{in} as small as possible. Figure 2 shows the ratio between the crystalline particles detected N_D by the order parameter in the first layer and the total number of particles in the template as a function of r_{in}. The inset shows how the order parameter performs if the first layer is filled with 1000 different configurations of randomly disposed particles. We have chosen r_{in} so that at least 90% of solid particles are correctly detected. With this setup, only 5% of the randomly positioned particles are recognized as crystalline. Figure 3 shows a typical snapshot of crystallites forming on the **100** and **111** templates.

Crystals growing on the **100** and **110** templates are straightforward to analyze with this order parameter as the stacking is unique. A bit more care is required in the case of the **111** template as it has three distinct positions for the first layer and two choices for any subsequent layer (see Fig. 4). To reduce "false positives" due to fluid particles that happen to be close to a lattice site, we impose that particles will not be considered crystalline if they do not have at least two crystalline neighbors in the previous layer.

With this scheme to detect crystalline particles, we analyzed the size distribution of crystallites induced by the dif-
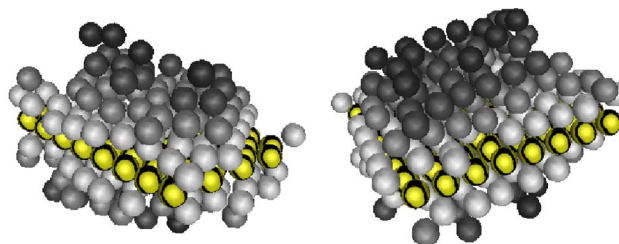

FIG. 3. (Color online) Snapshots of **111** (left-hand side) and **100** (right-hand side) templates. The particles that belong to the template have been highlighted by a black circular border. The grey spheres represent solid particles crystallizing directly on the template. Darker grey labels represent crystalline particles in subsequent layers.
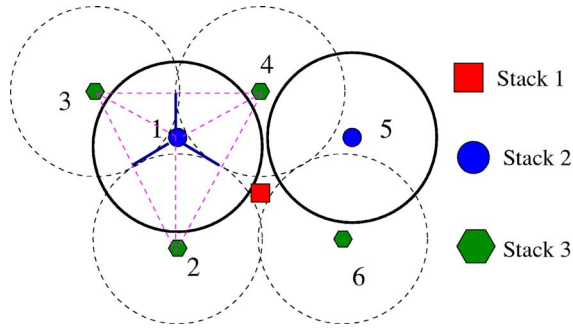
FIG. 4. (Color online) 111 template stackings.

ferent templates, as a function of the lattice constant a of the template and of the volume fraction of colloids in solution, η.

III. RESULTS

In a first simulation, we studied how the number of particles in an epitaxially grown crystallite (N_S) depends on the size of the template (expressed by N_T, the number of particles in the template). To this end, we considered a system of hard spheres at coexistence ($P^*=11.56$, $\eta=0.494$). Under these conditions, we should not expect to observe spontaneous bulk crystallization. For templates of four different sizes, we computed $P(N_S)$ as a function of N_S. Results are shown in Fig. 5. As the figure shows, curves for different template sizes do not superimpose. Hence the average size of the epitaxially grown crystal is not simply proportional to the area of the template. Clearly, larger templates are more effective in producing crystalline particles. The curves in the insets show how the ratio $(N_S/N_T)^{\max}$, corresponding to the most likely value of N_S shifts with the number of particles in the template N_T. This result is not immediately obvious as at coexistence there is no driving force to form a bulk crystal. Hence, the crystallites only form because they wet the template. But, apparently, the thickness of the wetting layer is limited. To understand, at least qualitatively this behavior, we follow the approach exposed in Ref. [14]. Using this approach, we can approximate the surface free-energy density of a circular template of radius R_T. For convenience, we

assume that we can approximate the volume of the N_T crystalline particles that cover the substrate by a spherical cap of height z. At coexistence, the surface free-energy density can be approximated as

$$\Sigma = \gamma_{ls}[1 + (z/R_T)^2] + (\gamma_{sw} - \gamma_{lw}) + \gamma_0 e^{-z/z_0}, \qquad (2)$$

where γ_{fs}, γ_{fw}, and γ_{sw} are, respectively, the the fluid-solid, fluid-wall, and solid-wall, interfacial free energy densities. γ_0 and z_0 parametrize the effective repulsion between wall-solid and solid-fluid interface which is expressed by the last term of Eq. (2).

We should mention that the last term in Eq. (2) is strictly speaking only correct for flat surfaces with large z. A more microscopic description would be required when dealing with a small number of layers. This would greatly complicate the present analysis. However, as our aim is not to obtain a quantitative description of the simulation data, but rather to gain qualitative understanding of the relation between the size of the template and of the crystallite, we use the very simplified picture of Eq. (7).

The main difference with the analysis reported in Refs. [13,14] is the presence of the $(z/R_T)^2$ term which is due to the finite lateral size of the template. It becomes irrelevant in the $R_T \to \infty$ limit. By minimizing Eq. (2) with respect to z we obtain

$$z = \frac{R_T^2 \gamma_0}{2z_0 \gamma_{fs}} e^{-z/z_0}. \qquad (3)$$

This equation can be solved numerically to give a set of points describing the functional dependence of the cap height z and the template size (R_T^2) (see Fig. 6). A power-law fit to these points $z \sim (R_T^2)^\eta$ yields an apparent exponent $\eta \simeq 1/3$. Hence, to a good approximation, the number of induced solid particles $N_S = \rho_s V_{cap}$ per template area $A_T = \pi R_T^2 \propto N_T$ is expected to increase as $N_T^{1/3}$. This estimate is consistent with the value $\eta = 0.30(5)$. obtained by fitting the results of the simulations as shown in Fig. 5.

The ability of a template to induce crystal growth is, of course, sensitive to the quality of the template. To test this effect, we consider the effect of fluctuations in the position of the template particles on the size of the epitaxially grown crystallite (Fig. 7). This figure shows that the size of the
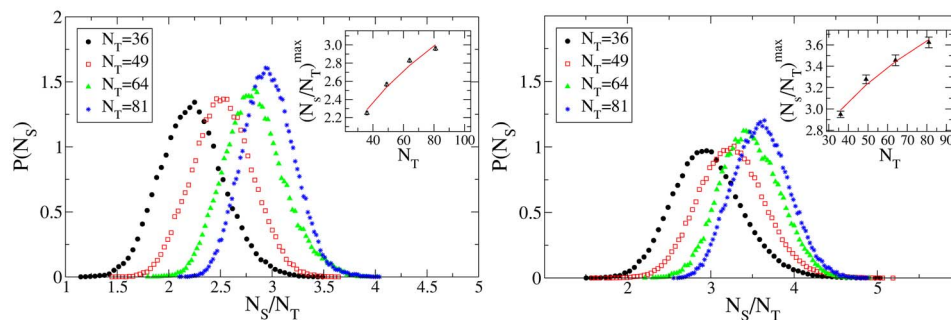

FIG. 5. (Color online) Probability distribution of finding N_S crystalline particles induced by templates **100** (left-hand side) and **111** (right-hand side) containing N_T particles as a function of N_S/N_T. The insets show how the ratio $(N_S/N_T)^{\max}$, corresponding to the peak of the distributions, depends on the number of particles in the template. Solid lines indicate power law fit to the data. All data have been taken at the equilibrium bulk lattice spacings of the respective crystals.
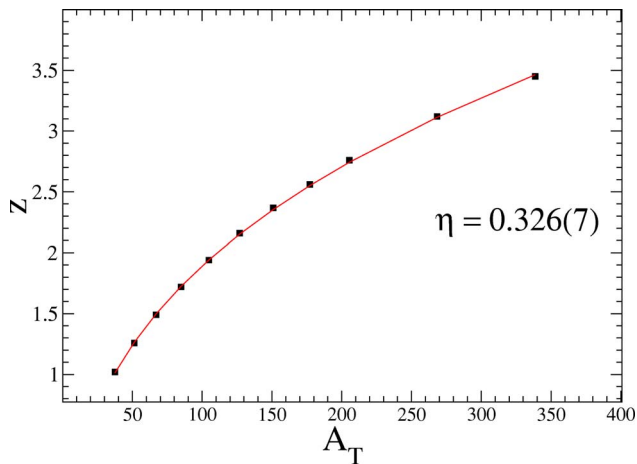
FIG. 6. (Color online) Plot and fit of the solutions of Eq. (3) as a function of the template area A_T. Here we used $\gamma_0=0.43 k_B T/\sigma^2$ and $z_0=2.5\sigma$ [13].

epitaxial crystal decreases when the templating particles are allowed to fluctuate around their lattice positions (both in and out of the template plane) under the influence of an harmonic potential,

$$V(\vec{r}(i)) = \frac{k}{2}(\vec{r}(i) - \vec{r}_0(i))^2. \tag{4}$$

Here k is the spring constant, $\vec{r}(i)$ is the position of the ith particle in the template, and $\vec{r}_0(i)$ is the lattice site the particle is bound to.

This harmonic potential mimics the experimental setup where template particles are fixed in space with optical tweezers. Figure 7 shows how the number of induced crystalline particles N_S decays with the average root-mean-square displacement (per lattice spacing) of the particles in the template. We call this quantity L_0. It is clear that as long as L_0 is contained to 0.05 the overall number of crystalline particles
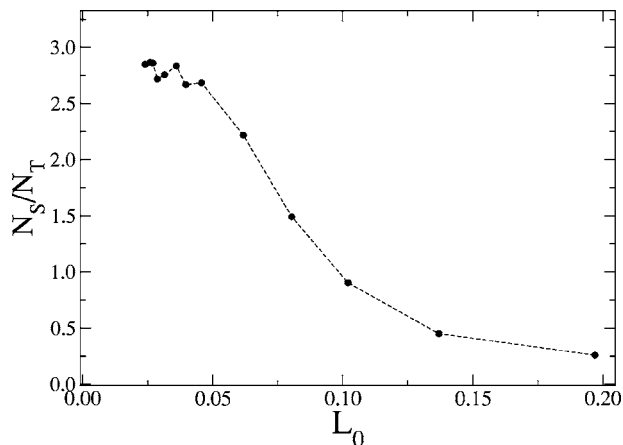

FIG. 7. Number of crystalline particles N_S induced by a template of area N_T particles as a function of the average root-mean-square displacement per lattice spacing of the particles in the template. This simulation has been carried out at $P^*=12.5$ for the **100** template with $N_T=64$.

induced by the template is unaffected. For larger values follows a rapid decay. It is interesting to compare these data to the empirical melting criterion due to Lindemann which states that a crystal melts when the root-mean-square vibration amplitude per lattice spacing exceeds 13% of the nearest-neighbor distance. From Fig. 7 we see that for this value $N_S/N_T \sim 0.65$ which means that when the Lindemann criterion is satisfied, the crystal cannot act as a substrate for crystal nucleation. It also implies that little is gained by reducing the rms displacement of template particles by more than 50% with respect to the Lindemann limit. Next, we consider the effect of a lattice mismatch between the template and the epitaxial crystal. To this end, we studied the variation of $P(N_S)$ with the template lattice spacing a at coexistence. Results are shown in Fig. 8. As expected [13,14] the optimal templates are those with a lattice spacing equal to the lattice constant a_{eq} of the stress-free equilibrium crystal. Making the spacing larger, decreases the quality of the template, but only slowly. However, decreasing the lattice spacing of the template quickly kills the tendency of the template to act as a seed. The dependence of the size of the epitaxially grown crystallite on the lattice spacing of the template is shown in the insets of Fig. 8. This observation suggests that if two crystals with different lattice spacing can grow on a template, a judicious choice of the lattice spacing of the template will make it possible to grow preferentially the crystal with the smaller lattice spacing. However, it will be difficult to select the crystal with the larger spacing.

As already noticed in Ref. [15], when the lattice spacing of the template is expanded even more than shown in Fig. 8, there comes a point where additional particles can occupy the vacancies in the template lattice. We explored to what extent each of the templates induces order within its own plane. We systematically examined lattice spacing ranging from $a=1.3\sigma$ to $a=2.4\sigma$ with an interval of $\Delta a=0.02\sigma$. We find that order is established in all template planes as soon as space is made to fit a particle in between. Figure 9 shows a density plot in the template plane (brightest spots correspond to the templating particles). In images **A**, **B**, **C** we can observe the restructuring inside the template layer when one particle can fit in between the templating particles, while images **D**, **E**, **F** in Fig. 9 show a density plot for lattice spacings that are large enough to accommodate more than one particle. For larger values of a the ability of the template to confine fluid particles in its interstitials decreases substantially but some residual order can still be found for slightly larger lattice spacings. These results are likely to be of practical importance given the practical restrictions on the total number of particles that can be trapped by the optical tweezers. The present results suggest that the number of template particles can be drastically reduced without affecting the quality of the template.

Thus far, we have only considered epitaxial growth at coexistence. The advantage of studying the system under those conditions is that the crystal formation is exclusively due to the template, as there is no thermodynamic driving force for bulk crystallization. However, in practice, experiments are always performed at finite supersaturation. It is therefore relevant to know how the tendency to grow epitaxial crystals is influenced by changing the osmotic pressure of the hard-sphere suspension.
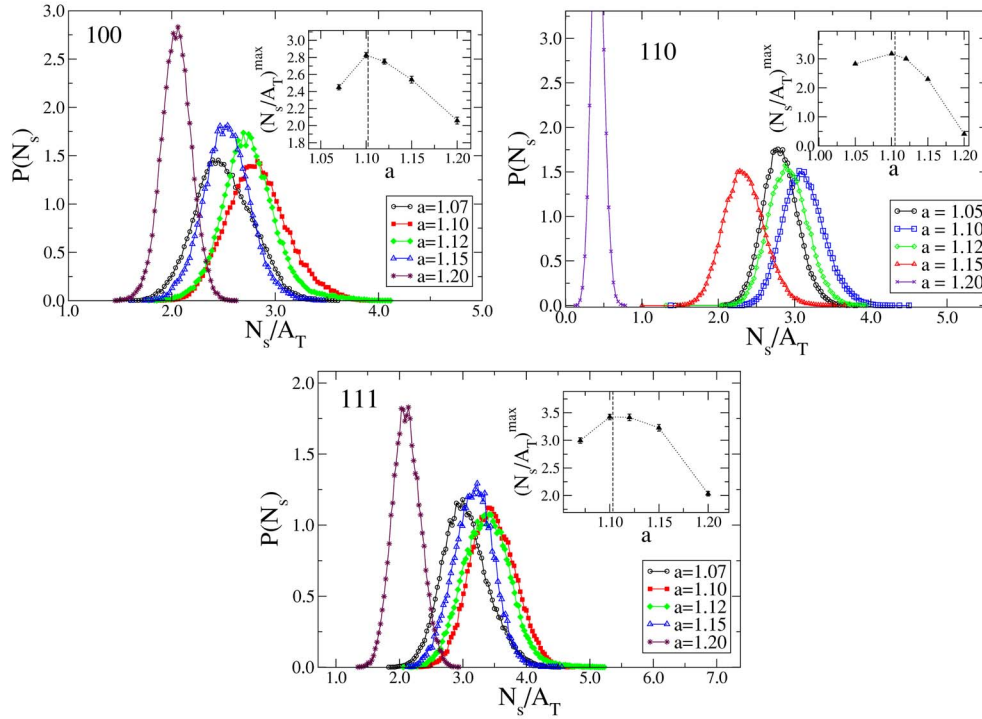
FIG. 8. (Color online) Probability distribution of finding N_S crystalline particles induced by templates **100**, **110**, and **111**, as a function of the lattice spacing a. The insets show how the ratio $(N_S/A_T)^{\text{max}}$ corresponding to the peak of the distributions depends on a.

It should be stressed that, as soon as the system is supersaturated, there is the chance that bulk crystallization will take place. However, this is an activated process. Hence, at moderate supersaturations, it is still possible to observe a finite (metastable) epitaxial crystallite. We measured the size of crystallites at different supersaturations for each template at their equilibrium lattice spacings with 64 particles. Figure 10 shows the results of this analysis. Higher pressures cause complete crystallization in the sample limiting our study to relatively small undercoolings. Notice how template **111**, which has the smallest interfacial free energy density [18] among the three templates, always induces a crystallite that is larger than the other two templates. In order to describe how the crystal size increases with the suspension's osmotic pressure P, we proceed as we did earlier by writing the Gibbs free energy of the system as

$$\Delta G = \gamma_{fs} S - |\Delta \mu| N_s + S \gamma_0 e^{-z/z_0}, \quad (5)$$

where S is the surface area of the nucleus and $\Delta \mu$ is the difference in chemical potential between the solid and the liquid. In our specific case we assume the shape of the nucleus to be a spherical cap (see Fig. 11). It follows that

$$S = S_{\text{cap}} = \gamma_{fs} \pi (z^2 + R_T^2), \quad N_s = \rho_s V_{\text{cap}} = \rho_s \frac{\pi}{6} z (3R_T^2 + z^2),$$

$$(6)$$

keeping only the z dependent terms we have

$$\Delta G = \pi z^2 - \rho_s |\Delta \mu| \left(\frac{\pi}{6} z (3R_T^2 + z^2) \right) + \pi R_T^2 \gamma_0 e^{-z/z_0}. \quad (7)$$

Minimizing Eq. (7) with respect to z we find

$$2z - \frac{\rho_s |\Delta \mu|}{2} (z^2 + R_T^2) = \frac{R_T^2 \gamma_0}{z_0} e^{-z/z_0} \quad (8)$$

which can be solved numerically for different values of $\Delta \mu$. Re-expressing $\Delta \mu$ in terms of the bulk pressure P we find that the P dependence of z can be fitted to a power law $z \propto P^{\eta}$ with $\eta = 1.9(1)$ (see Fig. 12).

This result shown in Fig. 10 shows that the simple analytical model accounts well for the numerical simulation data.

It is reasonable to assume that crystal nucleation at moderate undercooling can be described by classical nucleation theory (CNT). The Gibbs free-energy barrier to form a crystal nucleus composed of N_S particles surrounded by fluid can be expressed using Eq. (7). Ignoring the exponential term for large z we can find an analytical solution for the height of the critical spherical cap

$$z = R_0 [1 + \sqrt{1 + (R_T/R_0)^2}], \quad (9)$$

where $R_0 = 2\gamma_{fs}/(\rho_s |\Delta \mu|)$ is the CNT prediction for the radius of the critical nucleus in the absence of the template, and ρ_s is the equilibrium density of the crystal. Figure 13 shows the typical shape of free energy barrier as a function of the cap height z. Interestingly, the free energy as a function of z has a minimum for $z = R_0 [1 - \sqrt{1 + (R_T/R_0)^2}]$. This minimum corresponds to the thickness of the metastable, precritical crys-
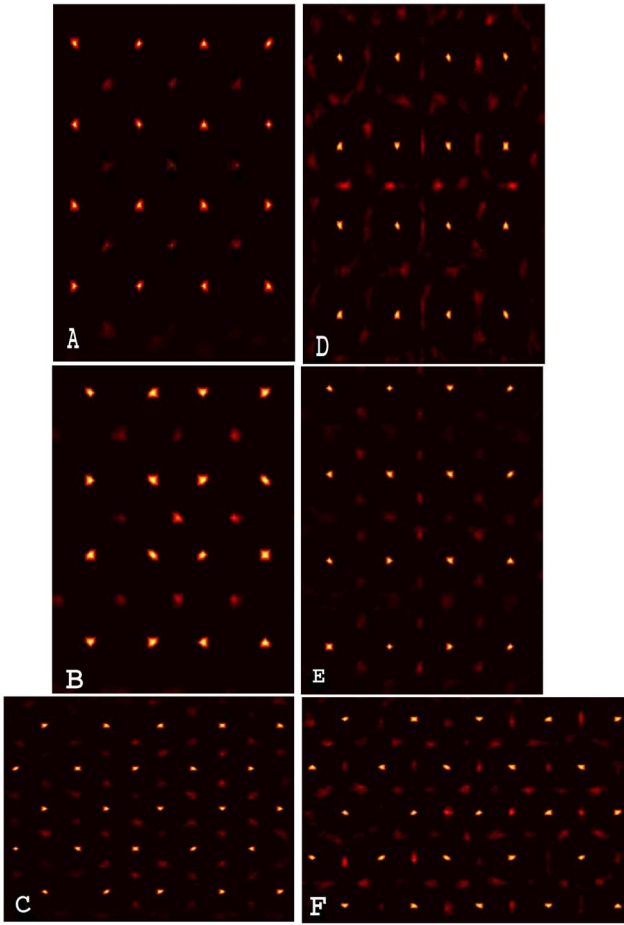
FIG. 9. (Color online) In-plane particle density plot. Bright spots correspond to the position of the center of the template particles. From top to bottom we imaged templates **100**, **110**, and **111**. The lhs corresponds to a lattice spacing large enough to accommodate one fluid particle in the template, namely (A) $a=1.48\sigma$ (**100**), (B) $a=1.48\sigma$ (**110**), and (C) $a=1.75\sigma$ (**111**). The rhs correspond to larger lattice spacings where additional particles could be inserted. (**D**) $a=2.14\sigma$ (**100**), (**E**) $a=1.76\sigma$ (**110**), and (**F**) $a=2.12\sigma$ (**111**). Data are averaged over 500 configurations.
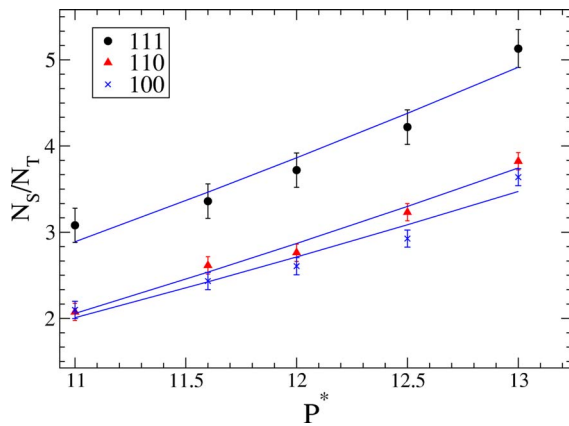

FIG. 10. (Color online) Peaks of the probability distribution of inducing N_S crystalline particles by templates **111**, **110**, and **100** containing N_T particles as a function of the system reduced pressure P^*.
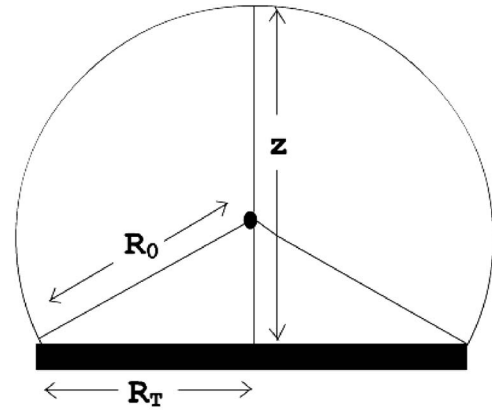

FIG. 11. Sketch of the assumed spherical cap shape forming over the template.

tallite that forms spontaneously on the template. The nucleation barrier corresponds to the free-energy difference between the critical nucleus and the metastable precritical crystal. Hence, the presence of the metastable crystallite has the effect to increase the nucleation barrier compared to that expected in the presence of a bare substrate [19].

We used this simple theoretical model to predict the pressure dependence of the nucleation rate. Of course, in a Monte Carlo simulation, we do not really compute rates. Rather, we know from earlier numerical studies of hard-sphere crystal nucleation that complete crystallization can take place on the time scale of a simulation, once the nucleation barrier is less than $\sim 15 k_B T$ [20] (the actual value depends weakly on system size). We therefore expect to observe spontaneous crystallization on a template at an excess pressure such that $\Delta G \sim 15 k_B T$. We can estimate ΔP if we insert $\Delta G = 15 k_B T$ in Eq. (7) and solve for $\Delta \mu$. Figure 14 shows the result that we obtain for **111** templates of different size. In all cases, we have assumed that $\gamma_0 = 0$. As can be seen from the figure, the simple analytical model accounts surprisingly well for the simulation data.

IV. CONCLUSIONS

To summarize, we have used Monte Carlo simulations to investigate the effect of crystallization templates, consisting
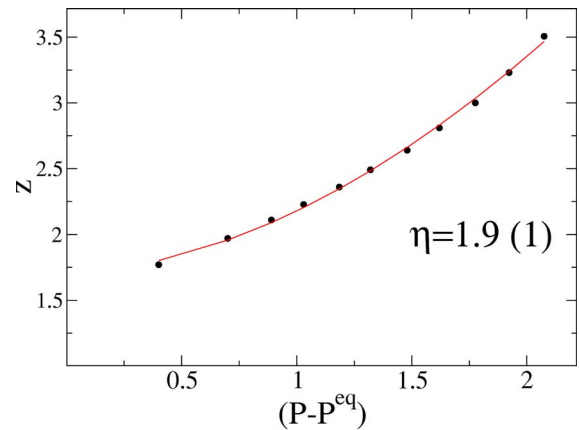

FIG. 12. (Color online) Plot and fit of the solutions of Eq. (8) as a function of the bulk pressure P minus the equilibrium pressure.
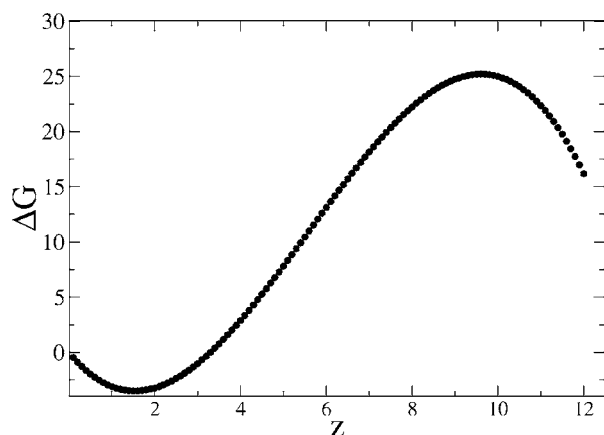
FIG. 13. The right-hand side shows a typical Gibbs free energy barrier of a system of hard spheres in the presence of a patterned substrate as a function of the spherical cap nucleus height.
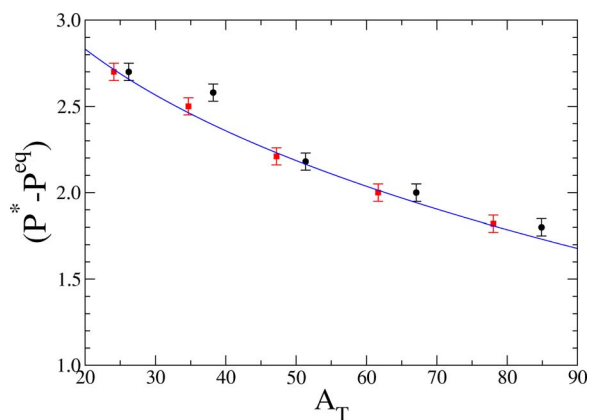

FIG. 14. (Color online) Crystallization onset pressure P minus the equilibrium pressure as a function of the template size. The squares shows the theoretical values (error bars take into account the uncertainty in the estimate of γ taken from Ref. [18]) and the circles the numerical data. The solid line is a guide to the eye.

of hard, colloidal spheres, on the growth of crystals from solution. We found that, for a given number of template particles, the **111** template is most effective in inducing epitaxial crystal growth. The size of the crystallites that form on the templates at coexistence are not simply proportional to the template area. However, a simple "wetting" picture accounts for the observed relation between template area and crystallite size. We find that disorder in the template can suppress its effectiveness, provided that the rms displacement of the template particles from their lattice sites is comparable to that specified by the Lindemann criterion (∼10% of the nearest-neighbor distance). However, if the disorder is a factor 2 less, the template is almost 100% effective. By introducing a lattice mismatch between the template and its target crystal, we can suppress crystal growth. However, the effect of lattice mismatch is much stronger for compressed templates than for expanded templates. We find that a simple modification of classical nucleation theory accounts well both for the size of metastable adsorbed crystallites at finite supersaturation and for the observed pressure dependence of the nucleation rate.

ACKNOWLEDGMENTS

[1] S. Chang, L. Liu, and S. A. Asher, J. Am. Chem. Soc. **116**, 6739 (1994).

[2] P. L. Flaugh, S. E. O'Donnell, and S. A. Asher, Appl. Spectrosc. **38**, 847 (1984).

[3] E. A. Kamenetzkv, L. G. Mangliocco, and H. P. Panzer, Science **263**, 207 (1994).

[4] H. B. Sunkara, J. M. Jethmalani, and W. T. Ford, Chem. Mater. **6**, 362 (1994).

[5] W. L. Vos, R. Sprik, A. van Blaaderan, A. Imhof, A. Lagendijk, and G. H. Wegdam, Phys. Rev. B **53**, 16231 (1996).

[6] I. I. Tarhan and G. H. Watson, Phys. Rev. Lett. **76**, 315 (1996).

[7] A. van Blaaderen, R. Ruel, and P. Wiltzius, Nature (London) **385**, 123 (1997); A. van Blaaderen and P. Wiltzius, Adv. Mater. (Weinheim, Ger.) **9**, 833 (1997).

[8] J. P. Hoogenboom, D. L. J. Vossen, C. Faivre-Moskalenko, M. Dogterom, and A. van Blaaderen, Appl. Phys. Lett. **80**, 4828 (2002).

[9] S. Ito, H. Yoshikawa, and H. Masuhara, Appl. Phys. Lett. **78**, 2566 (2001).

[10] S. Ito, H. Yoshikawa, and H. Masuhara, Appl. Phys. Lett. **78**, 2566 (2001).

[11] J. Won, T. Inaba, H. Masuhara, H. Fujiwara, K. Sasaki, S. Miyawaki, and S. Sato, Appl. Phys. Lett. **75**, 1506 (1999).

[12] C. Mio and D. W. M. Marr, Langmuir **15**, 8565 (1999).

[13] M. Heni and H. Löwen, J. Phys.: Condens. Matter **13**, 4675 (2001).

[14] M. Heni and H. Löwen, Phys. Rev. Lett. **85**, 3668 (2000).

[15] A. van Blaaderen, MRS Bull. **29**, 85 (2004).

[16] D. L. J. Vossen, A. van der Host, M. Dogterom, and A. van Blaaderen, Rev. Sci. Instrum. **75**, 2960 (2004).

[17] P. R. ten Wolde, M. J. Ruiz-Montero, and D. Frenkel, J. Chem. Phys. **104**, 9932 (1996).

[18] R. L. Davidchack and B. B. Laird, Phys. Rev. Lett. **94**, 086102 (2005).

[19] N. F. Carnahan and K. E. Starling, J. Chem. Phys. **51**, 635 (1969).

[20] A. Cacciuto, S. Auer, and D. Frenkel, Nature (London) **428**, 404 (2004).